Kinetic Studies of Superoxide Dismutases: Properties of the Manganese-Containing Protein from *Thermus thermophilus*§

Christopher Bull,† Eric C. Niederhoffer,‡ Tatsuro Yoshida,⊥,∥ and James A. Fee*,∥

Contribution from the Biophysics Research Division, The University of Michigan, Ann Arbor, Michigan 48109, and the Stable Isotope Resource, Isotope and Structural Chemistry Group (INC-4), Los Alamos National Laboratory, Los Alamos, New Mexico 87545.
Received August 20, 1990

Abstract: The catalysis of superoxide dismutation ($2O_2^- + 2H^+ \rightarrow H_2O_2 + O_2$) by manganese superoxide dismutase (MnSOD) from *Thermus Thermophilus* was examined by stopped-flow spectrophotometry. As found earlier by McAdam et al. [McAdam, M. E.; Fox, R. A.; Lavelle, F.; Fielden, E. M. *Biochem. J.* **1977**, *165*, 81–87], decay curves of O_2^- in the presence of MnSOD from *Bacillus Stearothermophilus* are characterized by three distinct phases: rapid disappearance of O_2^- (the "burst" phase), a period of approximately zero-order disappearance of O_2^- (the "steady-state" phase), and a very rapid depletion of O_2^- toward the end of the reaction. The enzyme from *T. Thermophilus* shows a similar kinetic pattern, and our data provide a chemical explanation for this behavior: The molar consumption of O_2^- in the burst phase is $([O_2^-]_B/[Mn]_T) \sim 80$. The magnitude of the burst is decreased ~2.5-fold in D_2O, whereas the zero-order phase is the same in both solvents. This indicates that proton transfer is probably the rate-limiting step when the enzyme is saturated with O_2^- and that the reaction by which inactive enzyme returns to active enzyme is not limited by proton transfer. At low temperatures (2–6 °C) in D_2O, the overall reaction was sufficiently slow to allow observation of spectral changes associated with the metal chromophore during the steady state, and we were able to obtain an absorption spectrum of the enzyme during this period. This was assigned to the inactive form of the enzyme and is characterized by a band near 650 nm ($\epsilon \sim 230$ $[Mn]^{-1}$ cm^{-1}) and a band near 410 nm ($\epsilon \sim 700$ $[Mn]^{-1}$ cm^{-1}). We speculate that inactivation of the enzyme occurs by oxidative addition of O_2^- to Mn(II), within a Michaelis complex, forming a cyclic peroxo complex of Mn(III) with the reverse of this reaction yielding active enzyme.

$$k_5 \sim 650\ s^{-1}$$

$$Mn^{II}{:}O_2^- \rightleftharpoons Mn^{III}{:}O_2^{2-}$$

$$k_{-5} \sim 10\ s^{-1}$$

A reaction scheme composed of a cyclic redox process, as described previously for the FeSOD of *Escherichia coli* [Bull, C.; Fee, J. A. *J. Am. Chem. Soc.* **1985**, *107*, 3295–3304], and the above reversible side reaction adequately account for the kinetic behavior of MnSODs.

In previous communications we described the steady-state kinetic properties of the iron-containing superoxide dismutase from *E. coli*,[1] of Cu/Zn-containing superoxide dismutase (SOD[35]) from bovine tissues,[2] and of FeEDTA.[3,35] In this paper we describe our studies with the manganese-containing protein from *Thermus thermophilus*.

There are three types of superoxide dismutases as determined by the metal involved in the catalysis of reaction 1: Cu, Fe, and Mn. The general properties, distribution, and possible biological

$$2O_2^- + 2H^+ \rightarrow O_2 + H_2O_2 \qquad (1)$$

function of these proteins have been discussed in a large number of review and discussion papers (cf. Ref 1 of ref 1 for reviews). The present work is concerned with manganese-containing superoxide dismutases, and the object of study is the protein from *Thermus thermophilus*. This protein is a tetramer of 21 kDa subunits, each of which binds, on the average, ~0.6 Mn(III) ions. Solutions of the protein have a reddish-purple color as the Mn(III) complex has an absorption maximum near 480 nm. Its three-dimensional structure has been described at a resolution of 2.4 Å.[4]

It is now widely held that metal ions catalyze reaction 1 by a cyclic redox process indicated by reactions 2 and 3. While a

$$M^{n+} + O_2^- \rightarrow M^{(n-1)+} + O_2 \qquad (2)$$

$$M^{(n-1)+} + O_2^- + 2H^+ \rightarrow M^{n+} + H_2O_2 \qquad (3)$$

number of transient and steady-state kinetic studies support this assertion, recent quantum chemical calculations based on the structure of the bovine Cu/Zn protein suggest that alternative schemes are possible.[5,6]

In the cases of Cu/ZnSOD and FeSOD, catalysis is described by a scheme in which enzyme–substrate intermediates are formed (Scheme I)

Scheme I

$$E_{ox} + O_2^- \underset{k_{-1}}{\overset{k_1}{\rightleftharpoons}} [E_{ox} - O_2^-] \xrightarrow{k_2} E_{red} + O_2$$

$$E_{red} + O_2^- \underset{k_{-3}}{\overset{k_3}{\rightleftharpoons}} [E_{red} - O_2^-] \xrightarrow{k_4} E_{ox} + H_2O_2$$

where protons are ignored. A general kinetic formalism has been derived for this scheme

$$-\frac{d[O_2^-]}{dt} = \frac{2[enz]TN[O_2^-]}{K_m + [O_2^-]} \qquad (4)$$

* Address correspondence to this author: Los Alamos National Laboratory, INC-4, Mail Stop C-345, Los Alamos, NM 87545.
§ Supported by U.S.P.H.S. Grant GM35189 (J.A.F.) and carried out under the auspices of the U.S. Department of Energy.
† Present address: Washington Research Center, W. R. Grace and Co., 7379 Route 32, Columbia, MD 21044.
‡ Present address: Department of Chemistry and Biochemistry, Southern Illinois University at Carbondale, Carbondale, IL 62901-4409.
⊥ Present address: Biophysics Group (P-6), Mail Stop K-480, Los Alamos National Laboratory, Los Alamos, NM 87545.
∥ Los Alamos National Laboratory.

(1) Bull, C.; Fee, J. A. *J. Am. Chem. Soc.* **1985**, *107*, 3295–3304.
(2) Fee, J. A.; Bull, C. *J. Biol. Chem.* **1986**, *261*, 13000–13005.
(3) Bull, C.; McClune, G. J.; Fee, J. A. *J. Am. Chem. Soc.* **1983**, *105*, 5290–5300.
(4) Stallings, W.; Pattridge, K. A.; Strong, R. A.; Ludwig, M. L. *J. Biol. Chem.* **1985**, *260*, 16424–16432.
(5) Osman, R.; Basch, H. *J. Am. Chem. Soc.* **1984**, *106*, 5710–5714.
(6) Rosi, M.; Sgamelotti, A.; Tarantelli, F.; Bertini, I.; Luchinat, C. *Inorg. Chem. Acta* **1985**, *107*, 121–122.

0002-7863/91/1513-4069$02.50/0

where [enz] = the concentration of enzyme active site metal, here $[Mn]_T$,

$$TN = [1/k_2 + 1/k_4]^{-1} \quad \text{(turnover number, } s^{-1}) \quad (5)$$

$$K_m = \frac{[1/k_2 + 1/k_4]^{-1}}{[1/k_r + 1/k_o]^{-1}} \quad \text{(Michaelis constant, } M) \quad (6)$$

$$TN/K_m = [1/k_r + 1/k_o]^{-1} \quad (k_{cat}, M^{-1}\ s^{-1}) \quad (7)$$

(which is traditionally the second-order reaction of the SOD protein with O_2^-)

$$k_r = k_1[k_2/(k_{-1} + k_2)] \quad \text{(rate of reduction, } M^{-1}\ s^{-1}) \quad (8)$$

and

$$k_o = k_3[k_4/(k_{-3} + k_4)] \quad \text{(rate of oxidation, } M^{-1}\ s^{-1}) \quad (9)$$

These expressions were found to accurately describe the kinetic behavior of bovine Cu/Zn[2] and *E. coli* FeSOD[1] under a wide variety of conditions. In each case, proton transfer from a general acid (H_2O) appears to be rate-limiting in the forward, first-order steps. In this work we provide evidence that the active Mn protein from *Thermus* probably operates by a very similar mechanism.

Previous work of McAdam et al.[7,8] with the MnSOD from *Bacillus thermophilus* and of Pick et al.[9] with the MnSOD from *E. coli* revealed that the manganese protein was kinetically more complicated than either Cu or Fe proteins. McAdam et al.[7,8] carried out a detailed study and interpreted their observations most simply in terms of a scheme involving a fast cycle and a slow cycle

$$E_{ox} + O_2^- \rightarrow E_{red} + O_2 \quad (10)$$

$$E_{red} + O_2^- \rightarrow E_{ox} + H_2O_2 \quad (11)$$

$$E_{red} + O_2^- \rightarrow E_C \quad (12)$$

$$E_C \rightarrow E_{ox} \quad (13)$$

in which E_C is an inactive form of the protein that spontaneously reverts to active enzyme, E_{ox}, but these were not otherwise defined. Nevertheless, this scheme, with proper values for the rate constants, rather closely emulated the observed behavior. By contrast, Terech et al.[10] failed to observe this behavior with the MnSOD from *Paracoccus denitrificans*.

Our kinetic data obtained with *Thermus* MnSOD are in full agreement with the occurrence of a dead end complex during catalysis. In this work we have expanded the kinetic scheme of McAdam et al.[7,8] to include substrate saturation, as observed with the other superoxide dismutases;[1,2] defined conditions to optimize formation of the dead end complex, and recorded the optical spectrum of this complex. By way of interpreting our data, we rely on a strong analogy between the mechanism of the Mn protein, in the fast cycle, with that of the Fe protein from *E. coli*.[1] We suggest, by analogy with model inorganic systems, that the dead end species results from the oxidative addition of O_2^- to Mn(II) to form a complex of Mn(III) and peroxide, $Mn^{III}{:}O_2^{2-}$, in which the peroxide is bound in a side-on fashion. We also show that kinetic analysis of these combined reactions accurately reflects the catalytic behavior of MnSODs.

Materials and Methods

T. Thermophilus cells were obtained from the American Type Culture Collection (No. 27 634), and the bacteria were grown as described previously.[11] The manganese superoxide dismutase was purified from the cytosol essentially as described by Sato and Nakazawa;[12] the concentration of active Mn was estimated from the visible absorption spectrum ($\epsilon_{480} = 910\ [Mn]^{-1}\ cm^{-1}$).

The three-syringe stopped-flow apparatus, the experimental techniques used to study catalyzed superoxide dismutation, and the processing of kinetic data have been described in great detail elsewhere;[1-3,13] these techniques were followed explicitly in this work, and the details of each experiment are described in the legends to the figures.

The stopped-flow apparatus was used as follows to detect the intermediate in the reaction of O_2^- with Mn^{II}EDTA in aqueous buffer.[14] One of the large syringes contained the metal complex (2.5 or 5 mM) in 10 mM MES/0.1 mM EDTA buffer at pH 6.5. The other large syringe contained 0.2 M $NaHCO_3$/0.1 mM EDTA pH 10; the final pH was ~10. A Me_2SO solution of 0.1 M KO_2/0.4 M 18-crown-6 was placed in the small syringe. The reagent solutions were maintained at 24 °C as was the mixing and reaction chambers. Two or three kinetic traces were averaged to obtain absorption values at 20-nm intervals in the 360–700-nm range.

Simulation of kinetic traces was carried out by numerically integrating relevant velocity expressions according to Gear's algorithm.[15]

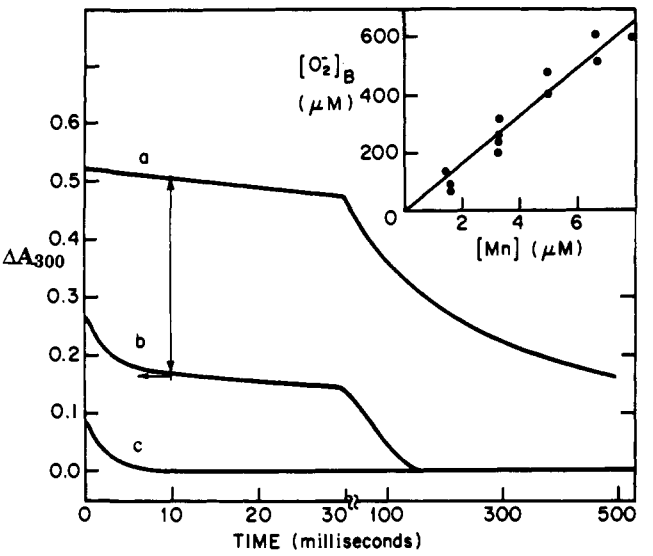

Figure 1. Demonstration of the burst in the presence of *Thermus thermophilus* manganese superoxide dismutase and analysis of its kinetic properties. The curves show the decay of absorbance at 300 nm due to the superoxide ($\epsilon = 284\ M^{-1}\ cm^{-1}$). Curve (a), no superoxide dismutase; curve (b), 6.7 μM MnSOD; and curve (c) corresponds to the data of curve (b) from which the steady-state catalysis of superoxide dismutation has been simulated and subtracted (see text). Note the change in time scale at 30 ms. The data of curve (c) are nicely fitted to an exponential function to yield the apparent rate constant, k_B, which corresponds to the transition of the enzyme from the active to the inactive form. The full amplitude of the burst $[O_2^-]_B$ is indicated by the double-headed arrow. Only a small amount of the burst can actually be observed in these decay curves (ca. the last 25%) due to the ~2–3-ms dead time of the stopped-flow apparatus.[1] The absorbance near the end of the burst (A*) was obtained from the single-headed arrow. *Experimental conditions*: optical pathlength = 2 cm; initial $[O_2^-]$ = 1 mM; [Mn] as MnSOD is indicated above; the buffer was 0.1 M AMPSO at pH 9.6 in H_2O; T = 2 °C. *Fitting parameters*: $\alpha = 170\ s^{-1}$, $\beta \sim 7$ μM, $k_B = 490\ s^{-1}$, amplitude of the burst = 0.56 mM. *Inset*: The size of the burst is proportional to the concentration of manganese superoxide dismutase present in the reaction mixture. The amount of superoxide consumed in the burst, $[O_2^-]_B$, was measured as the difference between the initial concentration of superoxide after mixing in the absence of enzyme and the concentration of superoxide immediately after the burst. The concentration of MnSOD is given as the concentration of protein bound Mn. The solid line corresponds to 80 superoxide ions consumed per Mn in the rapid phase of the catalytic reaction.

(7) McAdam, M. E.; Fox, R. A.; Lavelle, F.; Fielden, E. M. *Biochem. J.* **1977**, *165*, 71–79.
(8) McAdam, M. E.; Lavelle, F.; Fox, R. A.; Fielden, E. M. *Biochem. J.* **1977**, *165*, 81–87.
(9) Pick, M.; Rabani, J.; Yost, F.; Fridovich, I. *J. Am. Chem. Soc.* **1974**, *96*, 7329–7333.
(10) Terech, A.; Pucheault, J.; Rerradini, C. *Biochem. Biophys. Res. Commun.* **1983**, *113*, 114–120.
(11) Findling, K. L.; Yoshida, T.; Fee, J. A. *J. Biol. Chem.* **1984**, *259*, 123.
(12) Sato, S.; Nakazawa, K. *J. Biochem. (Tokyo)* **1978**, *83*, 1165–1171.
(13) McClune, G. J.; Fee, J. A. *Biophys. J.* **1978**, *24*, 65–69.
(14) Stein, J.; Fackler, J. P.; McClune, G. J.; Fee, J. A.; Chan, L. T. *Inorg. Chem.* **1979**, *18*, 3511–3519.
(15) Kahaner, D. K.; Sutherland, C. D. SDRVBI In *Common Los Alamos Mathematical Software Compendium*; Los Alamos National Laboratory, Los Alamos, NM, 1984.

Results

Conversion of Active-to-Inactive Enzyme. The only qualitative difference between the catalysis of reaction 1 by MnSOD and FeSOD appears to be the facile conversion of MnSOD, during catalysis, to an inactive form. The continuation of catalysis therefore depends on the rate at which an inactive enzyme reverts to an active form; this behavior is illustrated in Figure 1 (note change of scale at 30 ms). Curve (a) of Figure 1 shows the decay of O_2^- in the absence of enzyme. It is accurately described by the rate law for spontaneous dismutation

$$-\frac{d[O_2^-]}{dt} = k_1 + 2k_2[O_2^-]^2 \qquad (14)$$

as discussed previously.[1] Curve (b) shows the decay of O_2^- in the presence of MnSOD and is characterized by three distinct phases: First, a rapid but brief loss of superoxide, which occurs largely within the dead time of the instrument (~2–3 ms) under these conditions; this is the burst. This phase is due to active enzyme and its cessation is due to the buildup of inactive enzyme, as described previously by McAdam.[7] The burst is complete within ~10 ms after stop of flow.

The second phase is a steady state characterized by zero-order decay of superoxide. This is ascribed to the slow interconversion between inactive and active enzyme forms. Finally, there is a very abrupt depletion of superoxide, suggesting a high kinetic affinity of O_2^- for the active enzyme. The contribution of spontaneous dismutation is very small and easily accounted for in the velocity traces by previously described subtraction procedures (1). Curve (c) is generated by fitting of curve (b) *at times longer than 10 ms* in terms of expression 15, extrapolating to zero time, and

$$-\frac{d[O_2^-]}{dt} = k_1 + 2k_2[O_2^-]^2 + \frac{2\alpha[Mn]_T[O_2^-]}{\beta + [O_2^-]} \qquad (15)$$

subtracting the calculated values from the experimental data that yields curve (c) as a residuum. (The rightmost term in expression 15 is similar to expression 4 with α being analogous to TN and β to K_m; the relation between these symbols will be considered in the discussion. In this experiment, α = 168 s^{-1} and β = ~7 μM). Curve (c) was then simulated by using a simple exponential

$$A_{obs} = A^* e^{-k_B t} \qquad (16)$$

in which A^*, the "initial" absorbance, was obtained from the horizontal arrow in Figure 1. These manipulations of the data account quantitatively for the overall $A([O_2^-])$ vs time traces (cf. the exercise described in Figure 1 of ref 1).

Curve (c) of Figure 1 is thought to represent the shift of the system from operation of the fast cycle (Scheme I) to a steady state in which activity is determined by the rate at which the inactive enzyme returns to its active form.[7,8] As the dead time of the mixing system is not much less than the characteristic time of the inactivation process, we were only able to observe a small fraction of this reaction. The data obtained were consistent with an exponential process and yielded a specific rate constant which varied from ~330 to ~700 s^{-1}, with an average value around 650 s^{-1}, when the initial $[O_2^-]$ was increased from 1 to 5 mM. If, as suspected, the active enzyme is fully saturated at the high concentrations of O_2^- used here, then its conversion to the inactive form should be independent of O_2^- concentration.[2] While the data suggest some dependence of k_B on O_2^- concentration, the effect is very small, and, as a first approximation, we assume that conversion from active to inactive enzyme under our conditions is a first-order process having k_B ~ 650 s^{-1} (see Discussion).

The vertical arrow in Figure 1 corresponds to the molar consumption of O_2^- during the burst, $[O_2^-]_B$. The inset of Figure 1 shows that this increases linearly with the concentration of enzyme, and the slope of the solid line has a slope of ~80$[O_2^-]_B$/[Mn]; this ratio is a characteristic of the system under saturating conditions.

The Effect of D_2O on Active Enzyme. As shown in Figure 2, the magnitude of the burst was decreased by ~2.5 when the reaction was carried out in the presence of D_2O. Similarly,

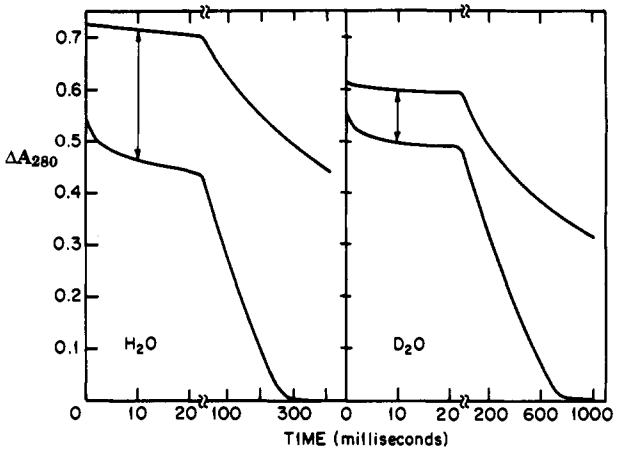

Figure 2. Deuterium isotope effects on the kinetic behavior of the manganese superoxide dismutase from *Thermus thermophilus*. The curves in both panels show the decay of absorbance at 280 nm due to superoxide (ϵ = 910 M^{-1} cm^{-1}). The upper traces were recorded in the absence of MnSOD, while the lower curves were obtained from experiments in which MnSOD was present. Each pair of traces (upper and lower) were recorded as close together in time as possible by using the same stock solution of superoxide. The arrows indicate the amplitude of the burst, which is ~2.5-fold smaller in D_2O than in H_2O. The observed rate constant associated with the burst, k_B, is not affected by the presence of D_2O while the α of the slow phase is decreased ~2.5-fold. Note the change in time scale at 20 ms. *Experimental conditions*: optical pathlength = 2 cm; initial $[O_2^-]$ was 0.4 mM in H_2O and 0.34 mM in D_2O; [Mn] as MnSOD = 1.4 μM in both experiments; the buffer was 0.1 M AMPSO at pH (pD) 9.3; T = 5.5 °C.

comparison of the steady-state regions led to the ratio of α_H/α_D = ~2.5. The decrease in the burst size is not due to an effect of D_2O on k_B, which is nominally the same in both solvents (data not shown), but rather to a slowing of the active enzyme. The value of β ranged from 3 to 7 μM and showed considerable variance in these experiments. Deuterium isotope effects on TN of a similar value have been observed with the Fe protein from *E. coli*[16] and with the Cu/Zn protein[2] where they were interpreted as indicating rate-limiting proton transfer to the active site. These observations suggest that the dismutation activity of MnSOD is limited by proton transfer under saturating conditions but that the conversion from inactive to active enzyme is not limited by proton transfer.

Reduction of Mn^{III}SOD by Peroxide. In our attempts to observe the inactive form of the enzyme (next section), it became important to consider the effect of high concentrations of peroxide in the reaction mixture. McAdam et al.[7] showed that H_2O_2 was able to reduce Mn^{III}SOD to Mn^{II}SOD. We studied this reaction in the stopped-flow instrument by observing the bleaching of the Mn^{III}SOD absorption, and the results afforded an interesting surprise. The initial velocity of the reaction, $\delta\Delta A_{480}/\delta t$, increased linearly with H_2O_2 over the range 2–12 mM, suggesting the first-order involvement of H_2O_2. Figure 3 shows a typical example of the raw data, ΔA_{480} vs time. We initially attempted to fit these data with exponential functions. This curve cannot be fitted with a single exponential, suggesting that it is not a pseudo-first-order process; attempts to fit with two exponentials left trends in the differences between experimental and computed data. It soon became apparent, however, that our hypothetical scheme (see below, Table I, Figure 7) predicted this should be a second-order reaction, and the data are adequately linear when plotted in reciprocal form (inset, Figure 3). The body of our data conform with a rate law (eq 17) that is second-order in Mn(III) and

$$-\frac{d[Mn(III)]}{dt} = k_{obs}[H_2O_2][Mn(III)]^2 \qquad (17)$$

(16) Fee, J. A.; Yoshida, T.; Bull, C.; O'Neill, P.; Fielden, E. M. In *Superoxide and Superoxide Dismutase in Chemistry, Biology, and Medicine*; Rotilio, G., Ed.; Elsevier Science Publishers: Amsterdam, 1986; pp 205–211.

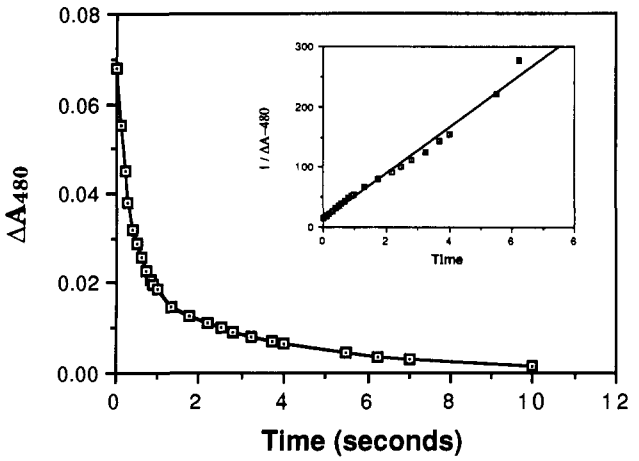

Figure 3. Reduction of $Mn^{III}SOD$ by H_2O_2. $\Delta A_{480}/2$ cm vs time is shown for the reaction of 42.5 μM $Mn^{III}SOD$ with 5.4 mM H_2O_2 in 0.1 M AMPSO buffer at pH 9.6 and 25 °C. The inset shows a standard second-order ($1/\Delta A$ vs time) plot of the data; the data for the first ~85% of the reaction are nicely linear, beyond this deviation occurs which does not appear to be systematic.

Table I. Velocity Expressions Used in Numerical Simulation of *Thermus* Manganese Superoxide Dismutase Kinetics[a]

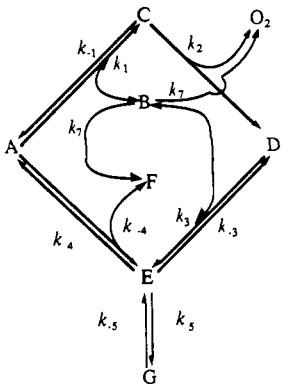

$$\dot{A} = k_4E + k_{-1}C - k_1AB - k_{-4}AF$$
$$\dot{B} = -k_1AB + k_{-1}C - k_3BD + k_{-3}E - 2k_7B^2$$
$$\dot{C} = k_1AB - k_2C - k_{-1}C$$
$$\dot{D} = k_2C - k_3BD + k_{-3}E$$
$$\dot{E} = k_3BD - k_{-3}E - k_5E - k_4E + k_{-4}AF + k_{-5}G$$
$$\dot{F} = k_4E + k_7B^2 - k_{-4}AF$$
$$\dot{G} = k_5E - k_{-5}G$$

[a] A = [$Mn^{III}SOD$], B = [O_2^-], C = [$Mn^{III}SOD{:}O_2^-$], D = [$Mn^{II}SOD$], E = [$Mn^{II}SOD{:}O_2^-$], F = [H_2O_2], G = [dead end complex]; the variation of each of these with time is indicated by a dot over the letter.

first-order in H_2O_2. This is consistent with a mechanism in which slow reduction of Mn(III) by H_2O_2 yields Mn(II) and free O_2^-, the latter reacting rapidly with another Mn(III) in the reductive half of the dismutation cycle (Scheme I). Because reaction of O_2^- with Mn(II) to form Mn(III) nulls the forward reaction (k_{-4}, see Table I), only k_r (eq 8) contributes to the observable, and thus, for each such event, two $Mn^{III}SOD$ are reduced to $Mn^{II}SOD$ (see below).

Spectral Observation of Inactive Enzyme. In the following experiments, we use the decreased turnover of the enzyme in the presence of D_2O to increase the time of the steady state and thereby facilitate observation of the dead end complex. Working at low temperature (5.5 °C) in the presence of D_2O, with $[O_2^-]_0$ of ~4–5 mM and ~40 μM MnSOD, we were able to observe optical absorption changes in the visible region of the spectrum while the enzyme was in steady state. (In all these experiments, absorbance is relative to absorbance at a very long time, e.g., 20 s.) A typical experiment is shown in Figure 4. In the upper panel, we are observing at 330 nm where the primary contributor to absorbance during the steady state is O_2^-. The linear portion of

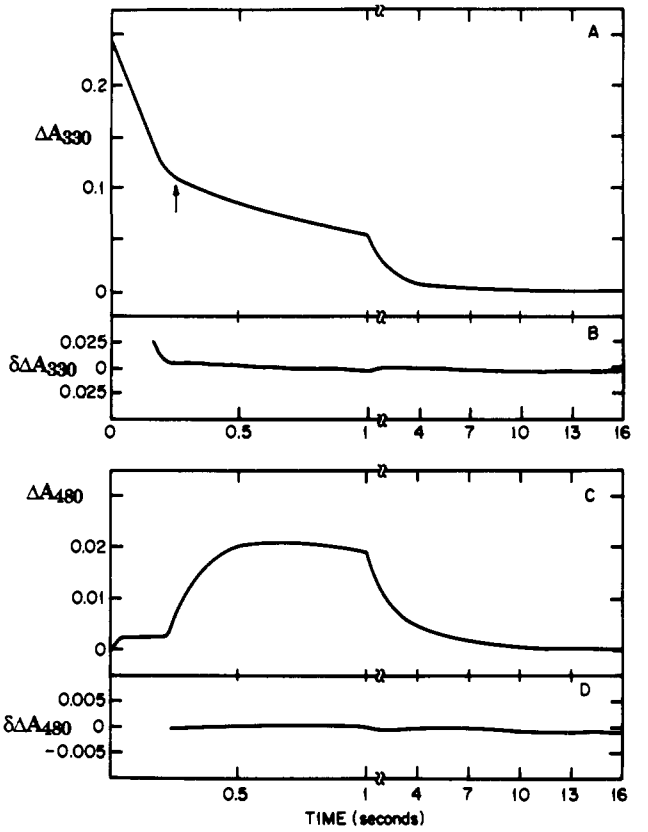

Figure 4. Direct observation of the manganese superoxide dismutase during catalysis. Panel (A) shows the changes in absorbance at 330 nm. In the early stages of the reaction, this is dominated by the decay of superoxide (ϵ = 33 M^{-1} cm^{-1}) which disappears in a zero-order fashion until it is effectively depleted at ~0.25 s as indicated by the arrow near the sharp break in the trace. Note time scale change at 1 s. The further decrease of absorbance at this wavelength is due to the combined relaxation of the system to the oxidized enzyme and its reduction by H_2O_2. Panel (B) shows the residuals obtained after fitting this process to a single exponential having an amplitude of 0.1 A at 0.25 s and a rate constant of 0.82 s^{-1}. Panel (C) shows the same reaction observed at 480 nm, where superoxide does not absorb but the oxidized protein absorbs maximally (ϵ = 910 M^{-1} cm^{-1}). After the superoxide is depleted, ~0.25 s, a rapid increase in absorbance occurs corresponding to the return of active enzyme followed by reduction of $Mn^{III}SOD$ by H_2O_2. Panel (D) shows the residuals resulting from a fit to two exponentials: The slow phase was fit to an amplitude of 0.027 A and a rate constant of 0.55 s^{-1}, while the fast phase was fit to an amplitude of 0.022 and a rate constant of 6.1 s^{-1}. *Experimental conditions*: optical pathlength = 2 cm; initial $[O_2^-]$ ~4–5 mM; [Mn(III)] as MnSOD = 41 μM; the buffer was 0.1 M CAPSO at pD = 9.8 in D_2O; T = 5.5 °C.

the decay curve indicates that we are observing the last ~0.25 s of the steady state, and the sharp break in the curve (arrow) is ascribed to depletion of O_2^-. Subsequent changes in absorption are due to the enzyme coming out of the steady state and equilibrating with the excess H_2O_2 in the reaction chamber. In the visible region, where the O_2^- has negligible absorption, one may observe changes ascribable to the metal chromophore of the protein. The lower panel of Figure 4 shows the absorbance changes which occur at 480 nm. In the steady-state region the absorbance is quite low as indicated by the flat portion of the kinetic trace between ~5 and 250 ms. At the end of the steady state a rapid increase in A_{480} occurs, and this is followed by a slower decay. The curve can be roughly fitted by two exponentials, and we ascribe the rise in ΔA_{480} (~6 s^{-1}) to the rate at which the enzyme returns to the active state and the decay of ΔA_{480} (~0.5 s^{-1}) to the apparent rate of reduction of Mn(III) enzyme by the excess peroxide. (It is unlikely that the second-order nature of the latter process would be perceived in these data.)

The ΔA in the steady state corresponds to the difference in absorption of the inactive enzyme and the enzyme after reaction with peroxide ($A_1 - A_{1=\infty}$). By measuring ΔA during this time

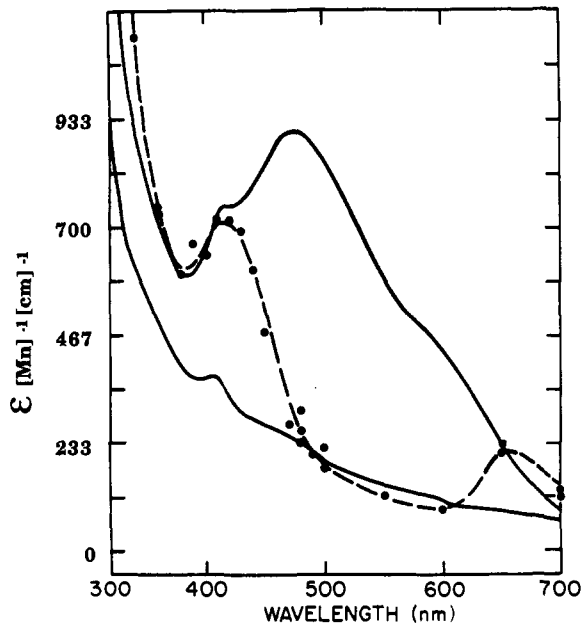

Figure 5. Spectrum of the inhibited state of manganese superoxide dismutase. The upper solid line corresponds to the absolute absorption spectrum of the oxidized protein, and the lower solid line corresponds to the absolute absorption spectrum of the peroxide-reduced form of MnSOD. The dashed line defines the absolute absorption spectrum of the inhibited form of MnSOD. Each absorption value (solid circle) was taken from one stopped-flow experiment in which the absorption of the intermediate (obtained at 0.25 s) was referenced to the peroxide-reduced protein (end of the reaction). These values were corrected for appropriate dilution factors, and optical pathlength then added to the absolute spectrum of the peroxide reduced protein.

period at several different wavelengths, it was possible to obtain the optical absorption spectrum of the inactive enzyme as shown in Figure 5. The upper solid line is the spectrum of $Mn^{III}SOD$, and the lower solid line is the spectrum of peroxide-reduced $Mn^{II}SOD$ as recorded in a standard spectrophotometer; each is expressed as absorbance per molar [Mn]SOD per cm. The ΔA_λ (per cm) obtained from the stopped-flow experiments were added to the spectrum of the peroxide-reduced protein to obtain the spectrum of the inactive enzyme; this is shown as the dashed line drawn through the solid circles.[3] The resulting absorption spectrum reveals a weak band near 650 nm ($\epsilon \sim 230\ M^{-1}\ cm^{-1}$) and a much stronger band near 410 nm ($\epsilon \sim 700\ M^{-1}\ cm^{-1}$); there are apparent isosbestic points with the spectrum of the oxidized protein near 370 and 400 nm.

Transients in the Reaction of MnEDTA with O_2^-. The optical absorption spectrum of the inactive MnSOD has a remarkable similarity to that of the green intermediate formed by reacting O_2^- with $Mn^{2+}EDTA$ in dimethyl sulfoxide;[14] that material has absorption bands near 580 and 430 nm. It is also reported[14] that reaction of aqueous solutions of $Mn^{II}EDTA$ with O_2^- in aqueous solution results in a transient having $\lambda_{max} \sim 620$ nm. We constructed the absorption spectrum of this transient species from stopped-flow measurements. This is shown in Figure 6 along with the spectrum of the dead end complex of $Mn^{III}SOD$ and that of the intermediate formed on reaction of O_2^- with $Mn^{II}EDTA$ in dimethyl sulfoxide.

Discussion

The three-dimensional structure around the metal binding site of the Mn protein from *T. thermophilus* is essentially identical with that of the Fe protein from *E. coli*.[4,17] Thus, each metal binds three histidines, one aspartic acid, one solvent molecule, and appears to have one unoccupied coordination position. In both cases, the metal binding site is surrounded by a hydrophobic shell

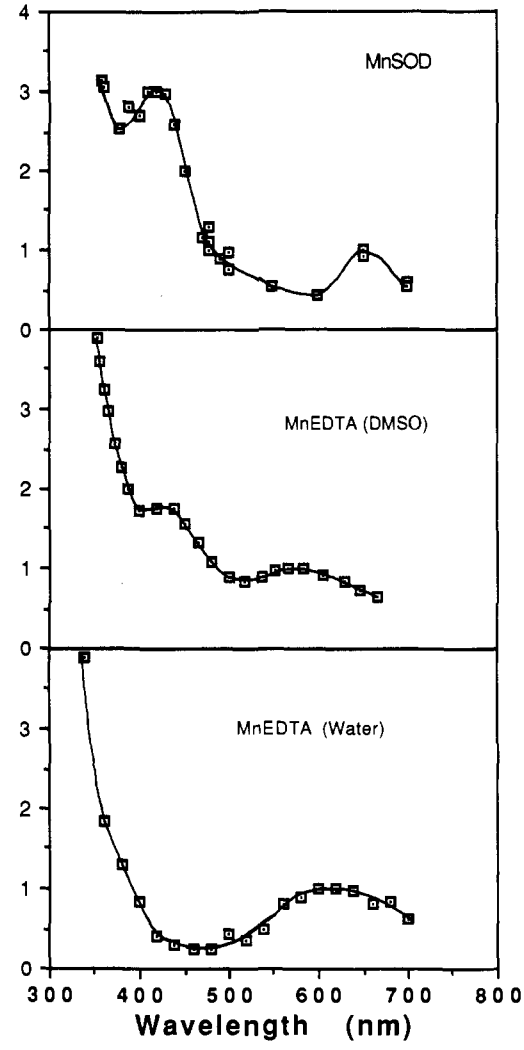

Figure 6. Comparison of the spectrum of the dead end complex with those of transient species formed in the reaction of O_2^- with $Mn^{II}EDTA$ in different solvents. Each spectrum is normalized to unit absorption at the long wavelength band. The upper curve represents the spectrum of the inhibited Mn protein, and conditions are as described in the legend to Figure 4. The middle curve is the absorption spectrum of the green intermediate which forms on mixing $Mn^{II}EDTA$ with O_2^- in Me_2SO and is taken from ref 14. The lower curve is the absorption spectrum of the transient intermediate formed on mixing $Mn^{II}EDTA$ with O_2^- in aqueous solution. The initial conditions were 1.25 mM or 2.5 mM $Mn^{II}EDTA$, 5 mM O_2^-, 0.1 M $NaHCO_3$; absorption data was taken at 50 ms after stop of flow.

consisting of several Phe, Tyr, and Trp residues prescribing a local region of low dielectric. The structure does not provide an obvious route by which O_2^- and protons can engage the metal center, but Ludwig et al.[30] have computed the accessible surface areas of the molecule and identified a small channel that appears to lead directly to the open coordination position on the metal. Alternatively, from Brownian dynamics simulation studies, Sines et al.[31] have suggested that Tyr-36 might flip out of the active site cleft allowing transient access of O_2^- to the metal.

A detailed steady-state kinetic study has been carried out on the Fe protein from *E. coli*.[1] The principal conclusions were that the enzyme is saturable above ~0.1 mM O_2^-, the value of TN is ~26 000 s^{-1} and is independent of pH, and the rate-limiting step under saturating conditions is transfer of protons from a general acid, probably H_2O, to a basic center that develops during catalysis. Given that Fe and Mn both have access to the II and III valence states and the near structural identity of the Fe and Mn proteins, it is reasonable that they should possess similar SOD mechanisms. While, this would not appear to be the case from a first look at the kinetic information, the essential identities in atomic structure and the underlying chemistry of superoxide

(17) Stallings, W. C.; Powers, T. B.; Pattridge, K. A.; Fee, J. A.; Ludwig, M. L. *Proc. Natl. Acad. Sci. U.S.A.* **1983**, *80*, 3884–3888.

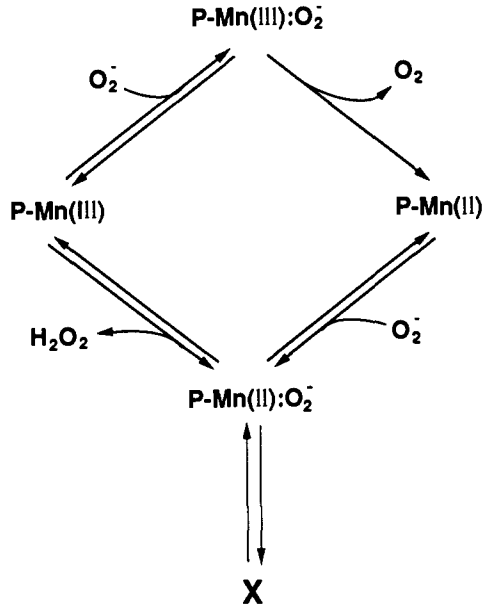

Figure 7. Proposed reaction scheme for MnSOD-catalyzed superoxide dismutation including two first-order rearrangements which lead from active to inactive and back to active enzyme. P = protein. Rate expressions are given in Table I.

dismutation suggest it must be so. Accordingly, we have interpreted present knowledge about the mechanism of the Mn protein in terms of the general scheme shown in Figure 7. In this scheme, the active form of the enzyme functions as predicted for the bacterial iron protein. The inactive enzyme arises by an internal rearrangement of the $PMn^{2+}:O_2^-$ complex to yield the inactive enzyme, X, which is speculated to be the side-on bound peroxo complex (see below). Active enzyme is regenerated by the decomposition of X to PMn^{3+} and peroxide. This scheme differs significantly from that proposed by McAdam et al.[8] (cf. reactions 10–13): (a) The inactive enzyme was previously thought to result from a bimolecular reaction between PMn(II) and O_2^-, whereas we suggest a first-order formation of inactive enzyme from a catalytically competent intermediate, $PMn^{II}O_2^-$. (b) They suggested that inactive enzyme was converted to the oxidized protein, while in the present scheme it is converted to the same intermediate in the catalytic cycle from which it was formed. Finally (c), their data gave "no clear indication of the detailed chemical changes involved in the slow cycle", while our data suggests a possible structure for the inactive enzyme.

Kinetic Analysis. We did not derive a steady-state velocity expression for the scheme in Figure 7. Instead, the differential expressions describing the scheme of Figure 7 were integrated numerically;[15] the velocity expressions are listed in Table I. Values for rate constants and for the experimentally determined extinction coefficients used in the numerical simulations are given in Table II. The rate constants, though not experimentally determined, are consistent with ours and others experimental data. Thus, O'Neill (personal communication) has measured k_r and k_o for *Thermus* MnSOD at 25 °C, finding values of 2.0×10^9 and 2.2×10^9 M^{-1} s^{-1}, respectively. Using expressions 6, 8, and 9, the constants in Table II predict $k_r = k_o = 3.9 \times 10^8$ M^{-1} s^{-1}, $k_{cal} = [(1/k_o + 1/k_r)]^{-1} = 1.95 \times 10^8$ M^{-1} s^{-1}, $K_m = 30.8$ μM, and TN = 6000 s^{-1} in D_2O at 5.5 °C. Similarly, $k_r = k_o = 6.25 \times 10^8$ M^{-1} s^{-1}, $k_{cal} = 3.12 \times 10^8$ M^{-1} s^{-1}, $K_m = 40$ μM, and TN = 12500 s^{-1} in H_2O at 2 °C. For comparison the experimental values of *E. coli* FeSOD at 25 °C and pH 8 are $K_m \sim 75$ μM, TN ~26000 s^{-1}, and $k_{cal} \sim 3 \times 10^8$ M^{-1} s^{-1}.[1,32]

To test the model against the derived velocity expression for Scheme I, we set k_5 and $k_{-5} = 0$ and generated traces analogous to the experimental data. For the conditions of Figure 1, we found, as expected, no burst phase, that the slope of the zero-order phase was equal to $2(1/k_2 + 1/k_4)^{-1}$, and that the derivative, $-d[O_2^-]/dt$, decreased to half its initial value at 40 μM O_2^-. The model thus predicts the qualitative behavior observed with FeSOD (see Figure 1 of ref 1), and the computed curves yield the kinetic parameters, TN and K_m, one would expect from plugging the individual rate constants of Table II into expressions 4–6.

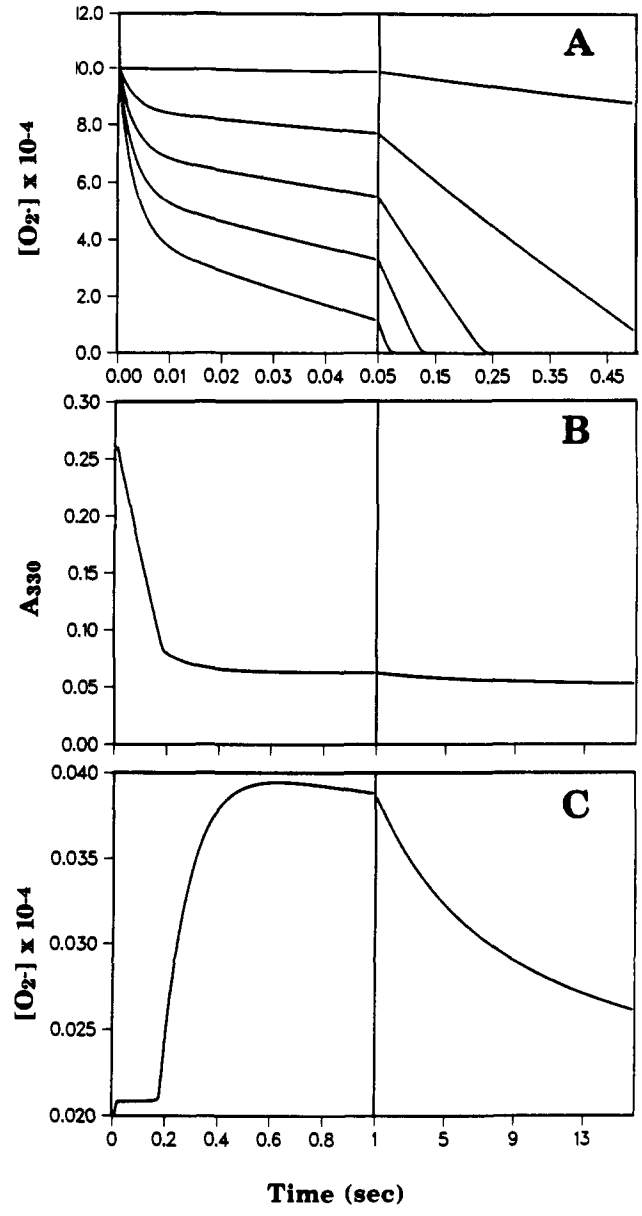

Figure 8. Simulation of the kinetic behavior of the proposed mechanistic scheme for manganese superoxide dismutases. Panel (A): calculation of $[O_2^-]$ as a function of time in the presence of 0, 2, 4, 6, and 8 μM Mn as MnSOD. The solvent is H_2O, the initial O_2^- is 1 mM, and the relevant rate constants used in the numerical integration are given in Table II. Panel (B) calculation of A_{330} vs time at high initial concentration of O_2^- and MnSOD. The solvent was D_2O, $[O_2^-]_o$ was 4.4 mM, and the rate constants and extinction coefficients are given in Table II. The extinction coefficient of superoxide at this wavelength is 33 M^{-1} cm^{-1}. The results of the simulation are computed for an optical pathlength of 2 cm and are directly comparable to the upper panel of Figure 4. Panel (C): calculation of A_{480} vs time. The conditions of analysis were as described for panel (B), and the results can be compared with the lower part of Figure 4.

By using the rate constants in Table II, we computed time traces for the two experiments of Figure 1 and of Figure 4; the results of this exercise are shown in Figure 8. Panel A shows the predicted behavior of the scheme relevant to the experimental results of Figure 1. Like the experimental data, the computed curves reveal a burst phase, an approximately linear segment, and a sharp break as O_2^- is depleted. At 20 ms the value of $[O_2^-]_B/[Mn]_T$ is 87, the α value calculated from the zero-order region is 360 s^{-1}, and the value of β is 3.6 μM. Fitting of the analogous experimental data, as described in the legend to Figure

Table II. Numerical Values of Rate Constants and Extinction Coefficients Used in Kinetic Simulations

rate constant	high enzyme, D_2O T = 5.5 °C pD = 9.8	low enzyme, H_2O T = 2 °C pH = 9.3
k_1 (M^{-1} s^{-1})	2×10^9	1.5×10^9
k_{-1} (s^{-1})	5×10^4	3.5×10^4
k_2 (s^{-1})	1.2×10^4	2.5×10^4
k_3 (M^{-1} s^{-1})	2×10^9	1.5×10^9
k_{-3} (s^{-1})	5×10^4	3.5×10^4
k_4 (s^{-1})	1.2×10^4	2.5×10^4
k_{-4} (M^{-1} s^{-1})	100	300
k_5 (s^{-1})	650	650
k_{-5} (s^{-1})	10	10
k_7 (M^{-1} s^{-1})	140	140
$[O_2^-]_o$ (M)	4.4×10^{-3}	1.0×10^{-3}
$[Mn]_T$ (M)	41×10^{-6}	1.0×10^{-6}

Extinction Coefficients

λ (nm)	330	380	410	480	650
oxidized protein ϵ ($[Mn]^{-1}$ cm^{-1})[a]	890	590		910	230
reduced protein ϵ ($[Mn]^{-1}$ cm^{-1})	590		400	230	170
intermediate ϵ ($[Mn]^{-1}$ cm^{-1})	1100	600	700	230	230

[a] [Mn] = molar concentration of active Mn.

1, with use of the velocity expression 15 gave values of $[O_2^-]_B/[Mn]_T \sim 80$, $\alpha \sim 170$ s^{-1}, and $\beta \sim 7$ μM. We also examined the time period in which the enzyme is being converted to the inactive form at different concentrations of O_2^-; there was no indication for a dependence of the rate of this conversion on the initial O_2^- concentration over the 0.2–2 mM range (not shown). This is consistent with the idea that X forms from the saturated enzyme.

According to the model, ~97% of the enzyme is in the inactive form during the steady state. Because the duration of the steady state is short compared to the time required to return from inactive to active protein, we presume the following relationship: $\alpha[Mn]_T = TN([Mn]_T - [Mn]_{inactive})$, where TN is the turnover number of the active enzyme. With the rate constants given in Table II, the fraction of active enzyme is ~3% giving TN ~5700 s^{-1}, which is lower by a factor of ~2 than the value of TN = 12 500 s^{-1} calculated from k_2 and k_4. Because the computed value of α is also higher than the experimental value by ~2-fold, the individual constants determining TN must be somewhat too large.[38]

The model suggests that β is not related to the K_m of the active enzyme. The calculated K_m for the active enzyme is 30–40 μM (depending on conditions), values similar to the K_m for *E. coli* FeSOD, and accordingly one would expect the velocity of the dismutation reaction to decrease as $[O_2^-] \approx K_m$; this is not observed in the computations. Rather, they show that as the system approaches the end of the zero-order phase, an increase in active enzyme occurs, which continues as the O_2^- is further depleted. Thus, during the end of the zero-order phase, the system is no longer in steady state and the sharp break in the curve is due to an increasing amount of active enzyme, rather than to an anomalously low K_m.

We also used the model to examine the reaction between peroxide and $Mn^{III}SOD$. Qualitatively, a plot of $1/[Mn^{III}SOD]$ vs time is perfectly linear over more than 90% of the reaction (not shown), and, because the subsequent reactions are so fast, the slope of the line is determined largely by the value of k_{-4}; a value of 500 M^{-1} s^{-1} is in reasonable agreement with the data of Figure 3. Importantly, this set of rate constants predicts that only ~0.1 μM (~0.25%) of the supposed peroxy complex will form; indeed we have no experimental evidence for the formation of this complex in the reaction of $Mn^{III}SOD$ with peroxide.

Panel B of Figure 8 shows the computed change in A_{330} and is directly comparable to the upper panel of Figure 4. There is reasonable qualitative concurrence between experiment and simulation. The initial A_{330} is similar in both experiment and computed data. The time at which O_2^- is depleted is at ~0.2 s in each case, and the absorbance at which the sharp break occurs is approximately the same in experimental and calculated curves. However, the detailed shape of the curve beyond the break is qualitatively different suggesting that additional events may be represented in the A_{330} data. This discrepancy may arise, for example, from the relative amounts of Mn(III) and Mn(II) that result from the decomposition of Mn^{II}–O_2^- (k_4 and k_{-3}); we have assumed a symmetric scheme, for which there is no a priori requirement.

For the experiment of Figure 4, the model predicts that the concentration of the dead end intermediate during the steady state is nearly constant at ~39 μM (95% of $[Mn]_T$) (not shown). Panel C of Figure 8 shows the computed change in A_{480} and is directly comparable with Figure 4. Here again, the qualitative time dependence agrees well with experiment. In particular, an increase of ~0.018 was observed at this wavelength, and an increase of ~0.019 is calculated. The length of the steady state follows a rough inverse proportion to the value of k_{-5}; here, we have used a value of 10 s^{-1}, which is somewhat larger than that estimated (~6 s^{-1}) from simulation of the rising portion of ΔA_{480} in Figure 4 (cf. ref 38).

In general, there is excellent qualitative agreement between the behavior of the scheme in Figure 7 and the observed behavior of the enzyme. The quantitative differences surely reflect the extreme difficulty of working with the very high concentrations of O_2^- (control of pH being a major difficulty), the different conditions used in our experiments, the simplistic assumptions reflected in the choice of rate constants, and possibly the occurrence of side reactions not accounted for in Figure 7. The model is not unique, but to a first approximation the concurrence between theory and experiment supports its validity as a working hypothesis.

The Nature of the Dead End Complex. There are three elements to the speculation that X of Figure 7 is a side-on bonded Mn(III)–peroxo complex: First, side-on bonded metal–peroxo complexes are easily formed, often very stable, and have been reported for a large number of metals (refs 18–27 and references therein). Second, the spectral properties of X are similar to those of known and suspected side-on peroxo complexes. According to Lever and Gray,[28] "the spectra of all these complexes, without exception, exhibit a weak absorption band ($\epsilon 10^2$–10^3 M^{-1} cm^{-1}) as the lowest energy identifiable charge-transfer feature. In some cases there is a shoulder or additional weak peak. This absorption is quite variable in position and may be in the near-infrared, visible, or ultraviolet region, depending upon the oxidation level of the metal ion". Accordingly, we assign the long wavelength absorption band to a LMCT from O_2^{2-} to Mn^{3+} for each compound; this fits the above criterion and favors the perception that these are side-on bonded peroxo complexes. Third, side-on peroxo complex formation is known to occur by oxidative addition of oxygen or superoxide to a low-valent metal, and this is facilitated by the absence of protons[18,29] (cf. also ref 3). The active site region of

(18) Vaska, L. *Acc. Chem. Res.* **1968**, *1*, 335–344.
(19) Valentine, J. S. *Chem. Rev.* **1973**, *73*, 235–245.
(20) Griffith, W. P. *J. Chem. Soc.* **1964**, 5248–5253.
(21) Griffith, W. P.; Wickins, T. D. *J. Chem. Soc. A* **1968**, 397–400.
(22) Hoffman, B. M.; Weschler, C. J.; Basalo, F. *J. Am. Chem. Soc.* **1976**, *98*, 5473.
(23) Newton, J. E.; Hall, M. B. *Inorg. Chem.* **1985**, *24*, 2573–2577.
(24) Van Atta, R. B.; Strouse, C. E.; Hanson, L. K.; Valentine, J. S. *J. Am. Chem. Soc.* **1987**, *109*, 1425–1434.
(25) Djordjevic, C.; Craig, S. A.; Sinn, E. *Inorg. Chem.* **1985**, *24*, 1281.
(26) Battacharjee, M.; Chaudhuri, M. K.; Purkyastha, R. N. D. *Inorg. Chem.* **1986**, *25*, 2354–2357.
(27) Norman, J. G., Jr.; Ryan, P. B. *Inorg. Chem.* **1982**, *21*, 3555–3557.
(28) Lever, A. B. P.; Gray, H. B. *Acc. Chem. Res.* **1978**, *11*, 348–355.
(29) McCandlish, E.; Miksztal, A. R.; Nappa, M.; Sprenger, A. Q.; Stong, J. D.; Spiro, T. G. *J. Am. Chem. Soc.* **1980**, *102*, 4268–4271.
(30) Ludwig, M. L.; Pattridge, K. A.; Stallings, W. C. In *Manganese in Metabolism and Enzyme Function*; Wedler, F. C., Schramm, V. L., Eds.; Academic Press: New York, 1986; pp 405–430.
(31) Sines, J.; Allison, S.; Wierzbicki, A.; McCammon, J. A. *J. Phys. Chem.* **1990**, *94*, 959–961.
(32) Fee, J. A.; McClune, G. J.; O'Neill, P.; Fielden, E. M. *Biochem. Biophys. Res. Commun.* **1981**, *100*, 377–384.
(33) Blakeley, R. L.; Dixon, N. E.; Zerner, B. *Biochim. Biophys. Acta* **1983**, *744*, 219–229.

MnSOD resides in an extremely hydrophobic environment prescribed by a shell of aromatic amino acid side chains surrounding the coordinated metal ion.[17] Thus, all the structural elements exist that would allow a peroxo complex to form from a transient $PMn^{II}:O_2^-$: oxidative addition occurring when a proton is not available, to form $PMn^{III}O_2^{2-}$, and electron transfer occurring when a proton is available. Cabelli and Bielski[34] may also have observed such a species as a transient in the reaction between $Mn(II)_{aq}$ and O_2^- in phosphate buffer.

Acknowledgment. We thank Dr. Peter O'Neill of the MRC Radiobiology Unit, Oxon, United Kingdom for measuring k_r and k_o of the *Thermus* MnSOD and for a careful reading of the manuscript and Ms. Carol Nettleton and Ms. Karen L. Findling for skillfully provided solutions of highly purified protein.

Registry No. D, 7782-39-0; Mn, 7439-96-5; H_2O_2, 7722-84-1; O_2, 11062-77-4; superoxide dismutase, 9054-89-1.

(34) Cabelli, D. E.; Bielski, B. H. J. *J. Phys. Chem.* **1984**, *88*, 6291–6294.

(35) Abbreviations: SOD, superoxide dismutase; Me_2SO, dimethyl sulfoxide; AMPSO, 3-*N*-((α,α-dimethylhydroxyethyl)amino)-2-hydroxypropanesulfonic acid; EDTA, ethylenediaminetetraacetic acid: MES, 2-(*N*-morpholino)ethanesulfonic acid; CAPSO, 3-(cyclohexylamino)-2-hydroxy-1-propanesulfonic acid.

(36) McAdam et al.[7,8] working under nonsaturating conditions, report a second-order rate constant of $\sim 3 \times 10^7$ M^{-1} s^{-1} for inactivation of the enzyme from *B. stearothermophilus* at 5 °C and very low O_2^- concentrations. While our stopped-flow instrument can measure rates as high as ~ 1000 s^{-1}, it does not allow us to measure $[O_2^-]$ much below 1 μM; thus making it impossible for us to determine the second-order rate of inactivation.

(37) Typically Mn(II) complexes have very weak absorption spectra in the visible region. We know from magnetic susceptibility experiments that the peroxide-treated protein is indeed in the Mn(II) valence state (Peterson, J.; Kent, T. A.; Fee, J. A.; Day, E. P., manuscript in preparation). It is likely that the apparent absorption of the reduced protein is due mostly, if not entirely, to Rayleigh scattering.[33]

(38) Within rather narrow limits (factors of ~2) it is possible to "fiddle" the values of the rate constants to achieve better fits to some of the experimental results but at the expense of producing greater variance with others. For example, the length of the steady state is very sensitive to the value of k_{-5} and somewhat less sensitive to k_2 and k_4. Similarly, $[O_2^-]_B/[Mn]_T$ is very sensitive to k_2 and k_4 and rather insensitive to k_{-5}, while the value of α is very sensitive to k_{-5}. Given the large number of rate constants and the relative paucity of experimental data, a complete sensitivity analysis would be premature.

(39) The model is useful for testing certain ideas about the physiological role of these proteins. Assuming concentrations of MnSOD and FeSOD of 10 μM within an *E. coli* cell and O_2^- flux rates ranging from 10^{-4} M s^{-1} to 10^{-9} M s^{-1}, we found no significant accumulation of inactive MnSOD in the absence or presence of FeSOD. Therefore, it is unlikely that a peroxo form of MnSOD ever forms under physiological conditions.